Nanotechnology Perceptions
ISSN 1660-6795
www.nano-ntp.com

Rational Design of Fe(II)−Polypyridyl Complexes for Applications of High Performance Dye-sensitized Solar Cells

Waleed S Alkhuraiji

Chemistry Division, Civilian Studies Department, King Khalid Military Academy (MNG), Riyadh - 11495, Saudi Arabia, wsikhraiji@sang.gov.sa

Herein we have demonstrated a series of Fe(II)-polypyridine based dyes to uncover the effect of anchoring group on their overall photovoltaic characteristics and electron injection efficiencies for their advanced DSSC applications. Though these dyes are inexpensive and environmentally safe and abundant in nature, however heavy use of these dyes is restricted by the sub-picosecond time scale is required for the photoactive state to occur the charge-separation at the dye-semiconductor interface is deactivated via the intersystem crossover (ISC) into low-lying photo-inactive states. It is crucial to produce Fe-based dyes with fast interfacial electron transfer (IET) that can compete with ISC events. This work investigates how anchoring groups viz. carboxylic acid, cyanoacrylic acid, cayano tetrazole, and cayano dithiocarboxylic acid influenced the IET rates in the dye TiO2 composites. For the investigation of the IET rates we have used (TiO2)15 and found that electron injection rates are quite faster with cyanoacrylic acid, cyano tetrazole anchoring groups. With (101) TiO2 anatase surface the dyes showed nice change separation which is crucial for electron injection. Evaluation of different parameters like band alignment, LHE, excited state like times, IET rates reveal that these engineered dyes are more efficient than the parent dye.
Keywords: Dye-sensitized solar cell, Fe(II)-polypyridines, anchoring groups, interfacial electron transfer, density functional theory.

1. Introduction

The quest for sustainable and renewable energy sources has driven significant research and development of advanced materials for solar energy conversion [1, 2]. Among these technologies, dye-sensitized solar cells (DSSCs) have presented a promising avenue for the next-generation clean renewable solar energy sources due to their potential tuneable electronic structures, for low-cost production, versatility and relatively high efficiency under diverse lighting conditions [3-5]. In DSSCs visible light is absorbed by the dye, which then facilitates

interfacial electron transfer (IET) between the dye and semiconductor to convert sunlight into energy [6]. The most widely used semiconductor in these systems to date is TiO_2, and the typical sensitizers are Ru(II)-polypyridine complexes covalently bonded to the surface of nanoparticles through a carboxylic acid anchoring group [7, 8]. Central to the performance of DSSCs is the dye, which plays a critical role in light absorption and the subsequent generation of photoinduced electrons [9]. Due to their remarkable energy conversion efficiencies (η) above 11% under standard (Global Air Mass 1.5) lighting, DSSCs based on common metal organic complexes such as phthalocyanines, polypyridyl, and porphyrins have attracted a lot of attention thus far [10]. While traditional DSSCs have predominantly employed Zn porphyrin dye (13%), single organic dye (13.6%), and ruthenium-based-polypyridines dyes (11.5%) [11]. The high cost and limited availability of ruthenium have spurred interest in alternative materials. Iron (Fe)-based polypyridine dyes represent a compelling alternative due to their earth-abundance, low toxicity, also have favourable chemical and photo-physical properties [12].

$[Fe(bpy\text{-}dca)_2CN_2]$ (bpy-dca = 2,2′-bipyridine-4,4′- dicarboxylic acid) dye were first reported by Ferrere and Gregg and their photochemical studies revealed that these dyes have ability to sensitise TiO_2 semiconductors with carboxylic acid anchoring group [13]. Furthermore, these dyes showed band-selective sensitization from the originally excited short-lived metal-to-ligand charge transfer (MLCT) states, demonstrating that sensitization is feasible even though the absence of long-lived photoactive excited states [14]. Later on, the absorption properties of $[Fe(L)_2CN_2]$ (L = substituted 2,2′-bipyridine) on different solvents and derivatives are recorded and these data revealed that carboxylic acid anchor communicate to TiO_2 NPs more effectively than does phosphonic acid. Sensitization mechanisms was analysed by Meyer et al. and exposed two different mechanism for $[Fe(bpy)(CN)_4]^{2-}$-TiO_2 nano hybrid : first direct sensitization, in which excited electron from the Fe(II) centre is directly injected into Ti(IV) sites and second involving interfacial electron transfer (IET) from the dye's initially populated MLCT states into the TiO_2 conduction band known as indirect sensitization [14, 15]. Ru(II) chromophores showed photoactive metal-to-ligand charge-transfer (MLCT) states for hundreds of nanoseconds and experience interfacial electron transfer (IET) into the TiO_2 nanoparticle at near perfect quantum efficiency [16]. Therefore, compared to the Ru(II)-polypyridine sensitised solar cells, Fe(II)-polypyridine sensitised solar cells exhibit significantly reduced quantum efficiencies. This is because iron complexes have a weaker ligand field (a smaller t_{2g}-e_g gap) than ruthenium complexes. As a result, in Fe(II)-polypyridines, metal-centered (MC) ligand-field states have lower energies than the lowest energy metal-to-ligand charge transfer state [17].

Different groups had reported the ISC phenomena in the tren-based polypyridine model complexes $[Fe(tren(py)_3)]^{2+}$ and $[Fe(tren(6\text{-}Me\text{-}py)_3)]^{2+}$ [18] [19]. Clearly, the conflict between the ultrafast ISC event and the IET upon initial excitation of Fe(II)-polypyridines is the fundamental impediment to their employment as photosensitizers in photovoltaic assemblies [10]. As a result, knowing the different structural parameters that determine the overall ISC and IET rates are critical for rationally designing more efficient Fe polypyridine based dyes [13]. Anchoring groups that covalently link sensitizers to the semiconductor surface represent an important structural parameter that controls the kinetics of the IET transfer in DSSCs and were therefore chosen as targets for the modifications [20]. Replacing Ru(II) in

the polypyridyl dye with environmentally friendly and earth-abundant Fe(II) can further shrink the cost of DSSCs. Though Fe(II)-polypyridine complexes showed promising results, the use of Fe(II) based solar cell is limited as such devices encounter very low overall efficiency compared to the Ru(II)-based analogues. The major difficulty with the utilization of Fe(II) dyes in DSSCs is their low ligand field strength that results in the presence of a low-lying metal-centered state in these complexes and as a results of that after photo-excitation of the dye to a manifold of photoactive MLCT states, Fe(II)-based dyes undergo intersystem crossing (ISC) within a subpicosecond time scale. Thus the very short lifetime of the photoactive excited states make the biggest obstacle for the utilization of Fe(II)-polypyridines as a sensitizer in DSSCs.

The molecular design of Fe-polypyridine dyes is thus crucial for optimizing their performance in DSSCs. One of the key considerations in this design is the choice of anchoring groups, which facilitate the attachment of the dye to the semiconductor surface, typically titanium dioxide (TiO_2). The nature of the anchoring group not only affects the stability and binding strength of the dye but also influences the electron injection efficiency from the dye into the semiconductor. Various anchoring groups, such as carboxylates, cyanoacrylic acid, cyano tetrazole, and cyano dithio carboxylic acid have been explored to enhance the performance of Fe-polypyridine dyes in DSSCs. By systematically investigating the interactions between Fe-polypyridine dyes and TiO_2, we aim to elucidate the mechanisms by which anchoring groups influence DSSC performance.

2. Modeling and Methods of Computation:

Figure 1 displays the corresponding names and chemical structures of the examined dyes. For the donor-acceptor architecture Fe polypyridine complex is used as the donor and for the parent dye FD1, widely accepted carboxylic acid is used as anchoring group while Cyanoacrylic Acid, cyano tetrazole and cyano dithio carboxylic acid groups are modeled as anchoring groups for the rest of the dyes FD2-FD4. Eventually, we have selected the (101) periodic surface and the TiO_2 nanocluster as parts of the electron acceptor semiconducting material in the composite system with two distinct binding modes to investigate the electronic structure and kinetics of interfacial electron transfer [21, 22]. The particulars of these computations are given below.

2.1. Electronic structure calculations of the free dyes and dye-TiO_2 nanocluster composites:

Extensive experimental and theoretical investigations have examined the impact of cluster size on the interfacial electron injection process, and it has been demonstrated that smaller $(TiO_2)_{15}$ clusters can capture the realistic properties anatase structures [23]. We have selected the $(TiO_2)_{15}$ nanostructure to describe the interfacial electron transfer dynamics in dye-TiO_2 composite systems. Using the PBE1PBE hybrid functional, ground state geometry optimizations of the model dyes have been performed within density functional theory (DFT). Previous report suggests that such hybrid functional provides exact electronic properties that closely matches to the experimental ones. Localized 6-31+g(d) basis sets were applied to the lighter elements (S, C, N, O, and H) [24, 25] while LANL2DZP [26] basis sets with pseudopotential are employed for Ti metal. Time-dependent DFT (TD-DFT) computations

were used, using the lowest 30 singlet excitations, to get excited state attributes based on the ground state optimized geometry. Applying the Polarizable Continuum Model (PCM) [27, 28] using the integral equation formalism version in acetonitrile solvent as implemented in Gaussian 09 package [29] allowed for the incorporation of solvent effects (CH_3CN) in the TD-DFT calculations.

To determine the impact of various functionals on the excitations, we have evaluated the TDDFT calculations in a variety of hybrid functionals using a number of exchange correlation functionals, such as B3LYP [30], PBE1PBE, CAM-B3LYP, in conjunction with the 6-31+g(d) basis sets. Table 1 compiles the corresponding results of the two primary absorption peaks for FD1, and it shows that the experimental data is quite well reproduced by the PBE1PBE hybrid functional with 6-31+g(d) basis set. The auxiliary programmed package GaussSum 2.2.5 [31] was used to evaluate the major orbital contributions in order to interpret the nature of transition states.

Table 1: The effect of different hybrid functionals on the absorption peaks (λ in nm) of FD1 dye in acetonitrile solvent

Dye	B3LYP	CAM-B3LYP	PBE0	Expt. value
FD1	295, 321	296, 322	332, 392	275, 375,470

2.2. Electronic structure analysis of dye-TiO_2 (101) surface

In the present periodic simulation anatase TiO_2 (101) surface of 2 × 4 super cells with two-layer was created to form 2D periodic slab. All analysis used a periodic boundary condition (PBC) condition with a k-point sample of (1 × 1 × 1) of 10.224 Å × 22.6924 Å × 40.00 Å sizes. To avoid coupling between the adjacent layers, a 40 Å vacuum along the Z-direction was applied. ab initio simulation package Quantum Espresso was used to optimized by Perdew-Burke-Ernzerh (PBE) [32] functional with ultra-soft pseudo potential and generalized gradient approximation (GGA) [33]. 40 Ry was chosen as the cutoff energy for the plane-wave calculation. Bottom sheet atoms of the slab were settled down to their corresponding bulk positions and relaxation was done until force on each ion were diminished to < 0.01 eV/A.

2.3. Theoretical methodology for the interfacial electron transfer dynamics:

For all dye-TiO_2 nanocomposite systems interfacial electron transfer dynamics was examined using the extended Hückel (EH) model Hamiltonian formalism, which propagates the time-dependent electronic wave function, Ψ (t), with time [34, 35]. A more thorough justification of the quantum dynamical simulation technique is available elsewhere. In recent decades different methods for simulating molecular dynamics have been developed and showed quite accurate results with experimental observations. Tully's surface hopping [36], the stochastic Schrödinger equation, PYXAID program for nonadiabatic molecular dynamics [37], and density matrix propagation are the foundations for most of them [38]. We use a semi-empirical EH Hamiltonian in our approach, which allows us to determine the IET timescale. Moreover, systems of a thousand or more atoms can be accurately simulated utilizing this technique. The IET simulations of the dye-TiO_2 composite started with the EH particle states, which then evolved over time in accordance with the time-dependent Schrödinger equation. Survival probability P(t) is defined as the probability of the photoexcited electron will endure on the adsorbate dye at time t. The simulation of P(t) involves time-evolved electronic wave function

of the composite dye-semiconductor onto the dye's atomic orbitals for the simulation steps. Wave function for time-dependent formalism can be presented as a linear combination of atomic orbitals

$$|\Psi(t)\rangle = \sum_{i,\alpha} B_{i,\alpha}(t)\,|i,\alpha\rangle \quad \text{(a)}$$

where $|i,\alpha\rangle$, signifies the atomic orbital α of atom i. The required expansion coefficients $B_{i,\alpha}(t)$ merged in eq a can be subtracted according to

$$B_{i,\alpha}(t) = \sum_{i,\alpha} Q_{i,\alpha}{}^{q} C_q \exp[-(i/\hbar)\,\mathrm{E}_q\, t] \quad \text{(b)}$$

where Cq is the expansion coefficient of the initial state

$$|\Psi(0)\rangle = \Sigma_q C_q |q\rangle \quad \text{(c)}$$

The eigenvectors and eigenvalues Qq and Eq were gained by resolving the generalized EH eigenvalue problem, $HQ_q = E_q S Q_q$ (d)

Where H illustrates the EH Hamiltonian matrix and S is the atomic orbital overlap matrix

After obtaining time-dependent wave function, the survival probability was computed by the following steps:

$$P(t) = \left| \sum_{i,\alpha}^{MOL} \sum_{j,\beta} B_{i,\alpha}{}^{*}(t) B_{j,\beta}(t) S_{\alpha,\beta}^{i,j} \right|$$

(e)

where $S_{\alpha,\beta}^{i,j} = \langle i,\alpha \mid j,\beta \rangle$ and the indices α and β represents specific orbitals in atoms i and j, respectively. The excited electronic states of the adsorbate with strong electronic couplings to the semiconductor conduction band are used to determine initial states. Dye-$(TiO_2)_{15}$ was subjected to vacuum-based, with a step-size of 0.1 fs at frozen geometry simulation. The simulations of electron transfer dynamics for dye-$(TiO_2)_{15}$ composites were carried out at the optimized structure by PBE1PBE level of theory. Absorbing potential was applied to the bottom Ti atoms to prevent artificial recurrences in the electron transient populations. Finally, exponential functions were applied for fitting the simulated data to evaluate the survival probability.

3. Results and Discussion:

3.1 Electronic structures study for the free dyes:

The ground state optimized geometries of these dyes are shown in Figure 1. Table 1 represents the dihedral angles between donor and acceptor parts. In general, it is beneficial for a dye to maintain the co-planarity between the donor and acceptor group in order to facilitate the electron transfer process from the donor moiety to the semiconductor surface.

Table 2. Some specific dihedral angles of the optimized dyes

Name of the dye	Dihedral angle (degree) D-A
FD1	28
FD2	4
FD3	3
FD4	4

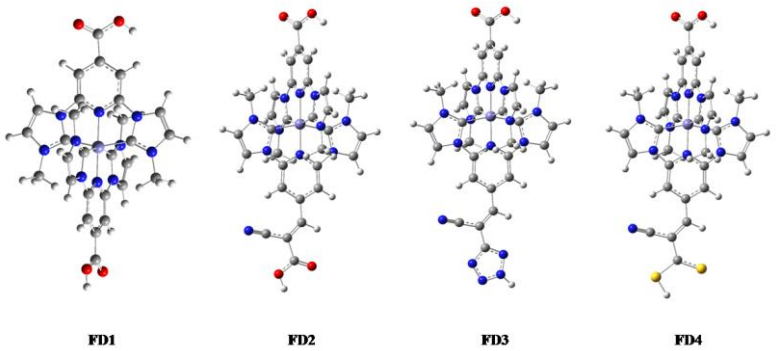

(a) (b) (c) (d)

Fig 1. Optimized ground state geometries of the dyes (a) FD-1, (b) FD-2, (c) FD-3, (d) FD-4 in acetonitrile solvent obtained at the PBE1PBE/ 6-31+g(d) level of theory.

It is revealed from Table 2 that the dye FD2-FD4 is more co-planar than the parent dye, indicating better electron delocalization and hence susceptible to better intra-molecular charge transfer. We have also analyzed the projected density of states of the individual dyes as illustrated in Figure 3. The donor part of the FD dyes (FD_D_PDOS) has a high contribution to the valence band of the overall dyes while the iron has high contribution to the conduction band of the dye system. Interestingly the contribution from the anchoring group for FD2-FD4 is denser than that for FD1.

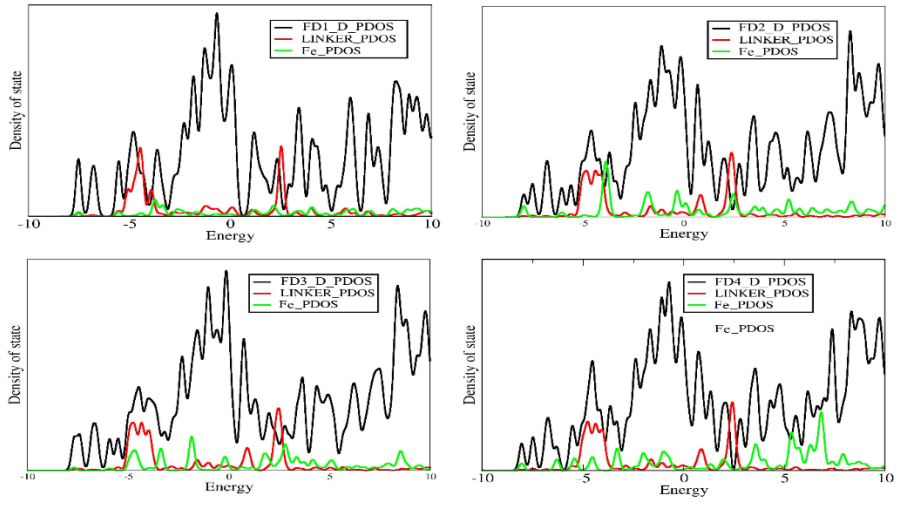

Fig 2. Projected density of states of the dyes (a) FD-1, (b) FD-2, (c) FD-3, (d) FD obtained at the PBE1PBE/ 6-31+g(d) level of theory.

3.2 Frontier MOs and Electron Injection Characteristics:

To account the influence of different anchoring groups on the electronic structures of the dyes, analyzed the nature of their frontier molecular orbital (FMOs). Selected orbitals like HOMO and LUMO of the dyes which are directly involved in the overall electron injection process of dye to semiconductor orbitals are shown Figure 3. For the HOMO, the electron density is equivalently distributed along the polypyridine unit, while the LUMO shows completely localized electron density over the anchoring groups of all the dyes. This type of situation is crucial to enhance the possibility of photo induced intramolecular charge transfer and ultimately electron injections happen from dye to the CB of TiO_2.

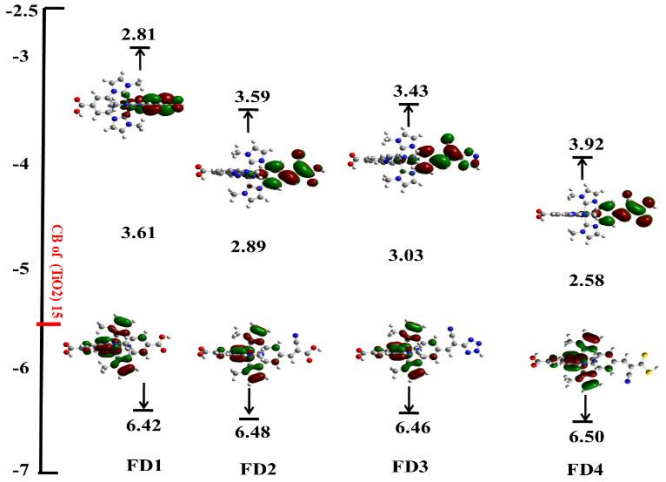

Fig 3. HOMO and LUMO levels isodensity plots for calculated energy levels of FD1- FD4 in acetonitrile solvent. The solid red line shows the CBM level of the TiO_2 (-4.0 eV)

HOMO, LUMO energy levels confirms that for all our investigated dyes LUMO energy levels are above the CB of TiO_2 (-4.0eV) while the HOMO levels are adequately deeper than the redox potential of I^-/I^{-3} system (-4.80eV). Such appropriate energy alignment of dye sensitizer with semiconductor ensure that all dyes can accomplish injecting electrons to the conduction band of TiO_2 while the regeneration of the excited dye is possible by unloading of electrons from I^-/I^{-3} electrolyte. Furthermore, LUMO energy levels of these dyes decreased with the incorporation of the model anchoring groups, while the HOMO levels of the dyes remain almost unchanged from FD1 to FD4. LUMO level stabilization markedly decreases the band gaps of the modeled dyes FD2-FD4 compared to the parent dye FD1.

3.3 Absorption and light harvesting characteristics:

Incorporation of anchoring groups in the dye system largely affects the photo-absorption behavior of the dyes. In order to obtain the absorption spectra of the dyes, FD1-FD4, we have applied TD-DFT calculations to get the light-harvesting efficiency data. In Figure 4 we have shown the simulated absorption spectra of all the dyes, having two major broad absorption band in the UV-visible region. Among the two major absorption bands of all the dyes, one is centering at around 280-330 nm and the other at around 450-515 nm (except FD1). The simulated absorption maxima that we have mentioned before, are in well agreement with our

experimental observation that anticipates two major absorption bands for polypridine-based dyes at 280 and 450 nm in acetonitrile solution. Remarkably, the longer wavelength bands correspond to intra-molecular charge transfer (ICT) transition, while the shorter wavelength bands are assigned to the localized aromatic π-π* transitions. In FD1, FD3, and FD4 molecules, π-π* transitions are more intense than ICT transitions, whereas FD2 molecules show the opposite trend. Furthermore, our dyes exhibited a substantially larger and red-shifted absorption band than the original FD1 dye, owing to better resonance with high co-planarity.

Table 3: Simulated absorption wavelengths (nm), oscillator strengths (f), and the composition of the corresponding electronic transitions (H = HOMO; L = LUMO), calculated in acetonitrile solvent by PBE1PBE/ 6-31+g(d) level of theory.

Dyes	λ_{max} (nm)	Oscillator strength (f)	LHE	% contribution
FD-1	392	0.2004	0.369	H-2->LUMO (17%), H-2->L+1 (26%), H-1->LUMO (38%), H-1->L+1 (11%) HOMO->L+3 (4%)
	332	0.1458		HOMO->L+2 (27%), HOMO->L+3 (61%) H-2->L+1 (5%), H-1->L+1 (3%)
FD-2	467	0.4109	0.612	H-1->LUMO (90%) H-2->LUMO (2%), H-2->L+1 (2%)
	283	0.6738		H-8->LUMO (94%)
FD-3	452	0.5003	0.684	H-1->LUMO (90%) H-2->L+1 (3%)
	301	0.2506		H-7->LUMO (47%), H-5->L+1 (16%) H-2->L+3 (7%), H-1->L+3 (9%), HOMO->L+3 (3%), HOMO->L+4 (7%), HOMO->L+5
FD-4	515	0.5203	0.698	H-1->LUMO (93%)
	311	0.4925		H-10->LUMO (85%) H-6->L+1 (5%), HOMO->L+4 (5%)

predominantly, FD3-FD4 have the highest harvesting capacities and the spectral coverage among the studied dyes. Furthermore, all the examined dyes have enhanced absorption intensity, or oscillator strengths, when compared to the mother dye. FD2-FD4 dyes had a significant red-shifting in optical absorption with a 35-45% rise in the molar extinction coefficient, which should lead to an increase in J_{sc} value and hence boost the conversion efficiency of DSSCs.

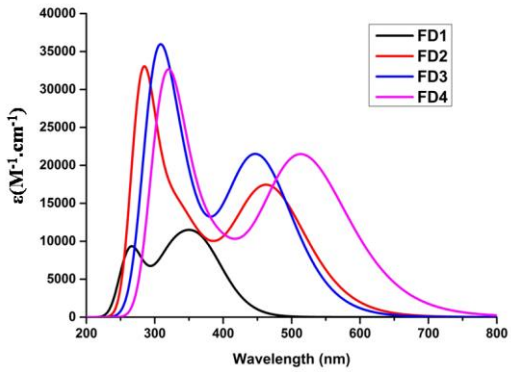

Figure 4. Simulated absorption spectra of FD1-FD4 at PBE1PBE/6-31+g(d) level in acetonitrile solvent.

Short circuit current (J_{sc}), is measured by the equation f, which is crucial to determine the overall efficiency of a solar cell

$$J_{SC} = \iint \frac{SI}{hc/e\lambda} LHE \times \phi_{inj} \eta_{coll} d\lambda dx \quad (f)$$

It can be argued from the above equation that J_{sc} is directly related to the electron-injection efficiency (φ_{inj}), light-harvesting efficiency (LHE) and the collection efficiency (η_{coll}). LHE is directly related to the absorption intensity by:

$$LHE(\lambda) = 1 - 10^{-f} \quad (g)$$

where f is oscillator strength related to molar absorption coefficient can be found from TD-DFT data [39, 40].

All of the model dyes have greater LHE values than the parent dye, particularly FD3 and FD4, which fall in the range of 0.612-0.698 (Table 2), indicating that these model sensitizers can provide a substantially larger photocurrent than the parent dye.

J_{sc} value is further related to the electron injection process (ΔG_{inj}) which can be simulated by

$$\Delta G_{inj} = E^*(dye) - |E_{CB}(TiO_2)| \quad (h)$$

where, E* (dye) presents the exited state oxidation potential of dye E* (dye) while E_{CB} (TiO_2) = - 4.0 eV for TiO_2 CB energy.

Exited state oxidation potential is expressed as $E^*_{dye} = E_{dye} - E_{0\text{-}0}$, where E_{dye} is the ground state oxidation potential of the dye assigned as a negative HOMO energy and $E_{0\text{-}0}$ presents vertical excitation. All the dyes except FD4 have negative ΔG_{inj} values (refer to Table 4), indicating that the electron-injection process is spontaneous involving FD1-FD3 dyes.

Table 4: Calculated electronic properties of FD1-FD4: the redox potential of the ground state of the dyes (E_{dye}), vertical transition energy ($E_{0\text{-}0}$), driving force of injection ($\Delta G_{in\,j}$) and the excited state lifetimes (τ) of the dyes.

Dyes	E_{dye} (eV)	$E_{0\text{-}0}$ (eV)	$\Delta G_{in\,j}$	τ(ns)	eV_{OC}
FD1	6.42	3.16	-0.74	10.35	1.19
FD2	6.48	2.65	-0.18	7.96	0.41
FD3	6.46	2.74	-0.29	6.12	0.57
FD4	6.50	2.41	0.09	7.64	0.08

Previous report confirms an analytical connection between V_{OC} and E_{LUMO} of the dyes

$$eV_{OC} = E_{LUMO} - E_{CB} \quad (i)$$

where (E_{CB}) is the CB of acceptor surface. This equation clearly demonstrated that the higher the value of E_{LUMO}, the larger that for V_{OC}. The simulated values of eVOC for the dyes are tabulated in Table 4.

3.4. Electronic structures of the Dye-TiO_2 interface:

To evaluate the photovoltaic properties of the dye-TiO_2 NPs composite systems we have chosen well known $(TiO2)_{15}$ and the corresponding ground state. Figure 5 presents the ground state optimized structures of the dyes@$(TiO2)_{15}$ nanocluster. Here the dyes bind to the nanocluster through a mono-dentate binding mode. From the geometric parameters it is clear

FD2 and FD3 yield shorter Ti-O bond compared to FD1 dye suggesting stronger bonding with $(TiO2)_{15}$ nano cluster. We have also analyse the projected density of states of the composite systems as shown in Figure 5. From the PDOS plot it is clear that the donor part contribute majorly to the valence band of the dye system while TiO_2 moiety contribute mostly to the conduction band of the composite system.

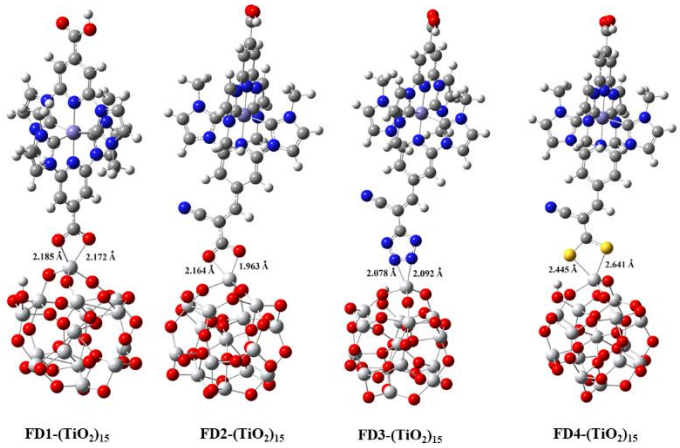

Fig 5. Optimized ground state geometries of the (a) FD-1@$(TiO2)_{15}$ (b) FD-2$(TiO2)_{15}$ (c) FD-3$(TiO2)_{15}$ (d) FD-4$(TiO2)_{15}$ obtained at the PBE1PBE/ 6 31+g(d)/LANL2DZ level of theory.

It is evident PDOS analysis (Figure 6) that all the dyes form a type-II band alignment with $(TiO2)_{15}$ cluster. The resultant band gaps for the FD2-FD3@$(TiO_2)_{15}$ composites systems are quite smaller than the parent FD1-$(TiO_2)_{15}$ composite, indicating that the formers interact the nanocluster much strongly than the latter one. The HOMOs are mainly localized in the donor region of the organic dyes, whereas the LUMOs lie mainly in the $(TiO2)_{15}$ cluster as shown in the Figure 7. The stronger interaction of the DF1 with respect to the FD1 can also be visualized from the red region of the interface of the electrostatic potential maps as illustrated in Figure 8.

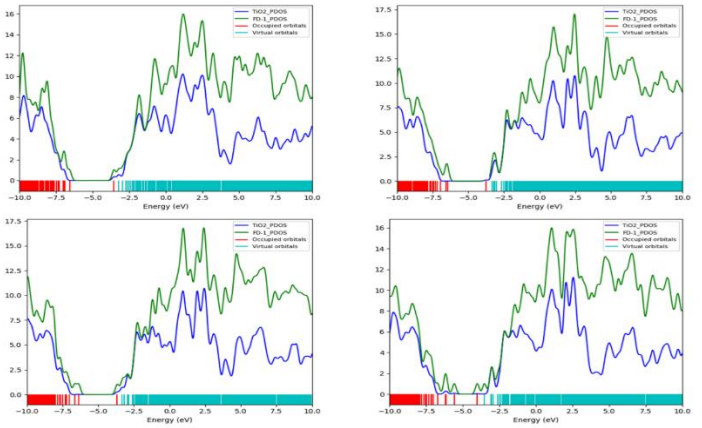

Fig 6. Projected density of states of the (a) FD-1@$(TiO_2)_{15}$ (b) FD-2$(TiO_2)_{15}$ (c) FD-

$3(TiO_2)_{15}$ (d) FD-$4(TiO_2)_{15}$

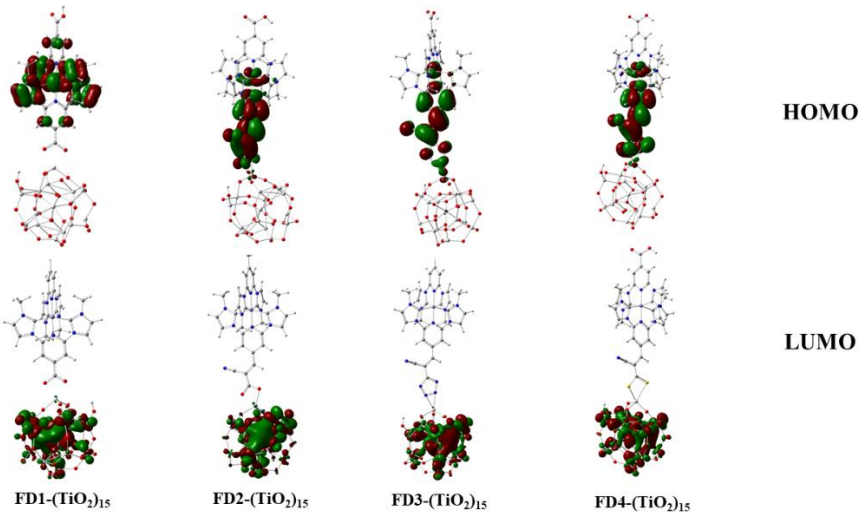

Figure 7. HOMO, LUMO isosurfaces plots of the FD-1@$(TiO_2)_{15}$, FD-2$(TiO_2)_{15}$, FD-3$(TiO_2)_{15}$, FD-4$(TiO_2)_{15}$ composites

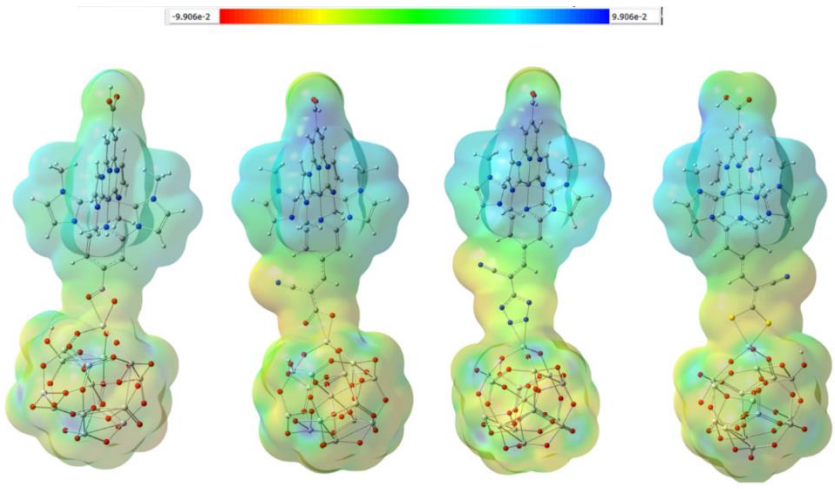

Figure 8. Electrostatic potential plots of the FD-1@$(TiO_2)_{15}$, FD-2$(TiO_2)_{15}$, FD-3$(TiO_2)_{15}$, FD-4$(TiO_2)_{15}$ composites

3.5. Simulation of interfacial electron transfer characteristic:

To set up the IET simulations the initial wavepacket is modeled by presenting electron into a LUMO orbital the excited of the dye obtained from EH formalism. Previous data confirms that this method is widely used to simulate across the semiconductor-dye hetero juncture. To get atomistic description of electron transfer time dependent Schrodinger equation (TDSE) was propagated within tiny, small-time intervals of 0.5 fs to 3000 fs. Time-dependent survival probability is denoted by P(t) at which electron resides in the dye complex for a time t. In IET

simulation time dependent survival probabilities of all FD1-FD4-$(TiO_2)_{15}$ nanocomposite are illustrated in Figure 7. The electron decay curves are fitted with the exponential equation j

$$f(t) = \exp(-t/\tau) \quad (j)$$

Interestingly IET plot clearly demonstrated that the photo-excited electron decays very slowly for FD1 (τ=14.92 ps) while for FD2 (τ=962fs) it decays very fast. Even for FD3 (τ=1.98 ps) and FD4 (τ=4.12 ps) the photo-excited electron decay is quite fast with respect to the parent dye FD1.

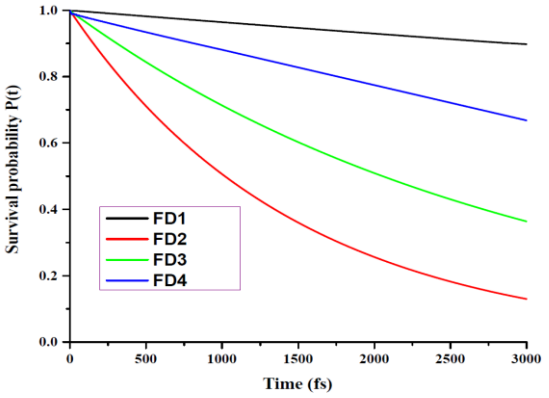

Figure 9. Time evaluated Survival probability plot for electron injection of FD–$(TiO_2)_{15}$ nanocomposites

Previous report revealed similar kind of observations for Ru(II)-polypyridine Complexes[35]. In order to explain these electron injection data, we have analyzed two most important parameters that are closely related to that heterojunction electronic coupling of the LUMO states of the dyes with the conduction bands of the semiconductor states viz. percentage of electron density on anchoring groups and the number of the state available for electronic coupling with the semiconductor acceptor states. The percentage of electron density on the different LUMO states of the dyes are analyzed and collected in Table 3. It can be argued that for FD2 and FD3 the LUMO, LUMO+1 and LUMO+2 orbitals offer the most electron density to the anchoring groups and for FD2 this density is maximum. Figure 9 represents the number of the LUMO states available for coupling with semiconductor acceptor states for FD1-FD4. For the MO energy level diagram, it can be seen that FD2-FD4 dyes possessed more dense LUMO states than that of FD1, which explain faster electron injection route for the former than the latter.

Table 5. Electron density (%) on the anchoring groups of FD1-FD-4 dyes

	% of Electron density on anchor			
Dye System	LUMO	LUMO+1	LUMO+2	LUMO+3
FD1	1	13	1	1
FD2	31	1	1	1
FD3	10	1	1	1
FD4	20	1	1	1

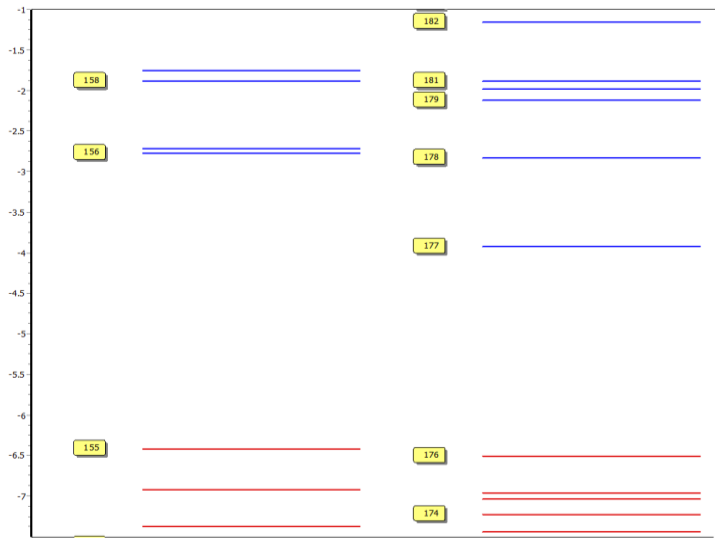

Figure 10. Energy level diagram of some selective free dyes FD1, FD2

3.6. Electronic structures of the Dye-TiO_2 periodic interface:

In order to determine the photovoltaic characteristics of the Dye-semiconductor composite system we have attached the individual dyes to the optimized anatase TiO_2 (101) surface and analyze the electronic structure of dye-semiconductor interface which is very crucial for predicting the overall performance of a DSSC. Interfacial electron transfer rates largely depend on the nature of binding mode of dye on semiconductor surface. Here we note that for all the dyes -TiO_2 composites bi-dented mode of attachment is the stable attachment as shown in Figure 11.

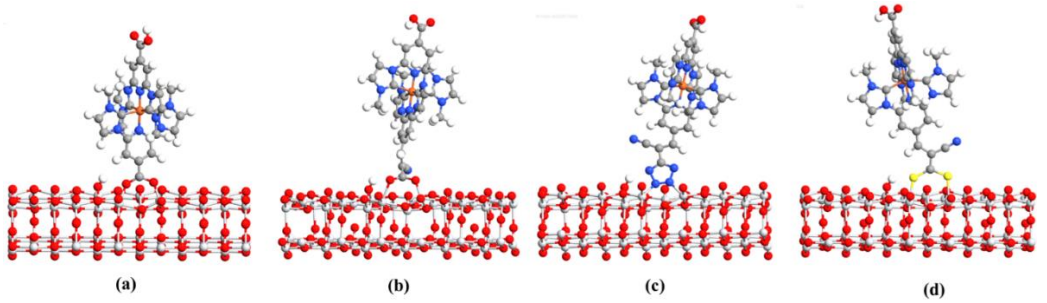

Figure 11. Ground state energy minimized geometries of the dyes adsorbed onto the TiO_2 (101) surface.

It is clear that The Ti-O bond lengths for dyes FD2-4 dyes on TiO_2 surface are shorter than the parent dye, indicating these dyes binds much strongly with the TiO_2 (101) anatase surface. Figure 12 represents the VBM and CBM states of the composite systems which reveal that HOMO is distributed over the dye part while LUMO is localized on the semiconductor part. Such a type of charge separation enhances the electron injection process. Importantly we found

comparatively large charge density on the anchoring groups of the FD2 dye with respect to other dyes.

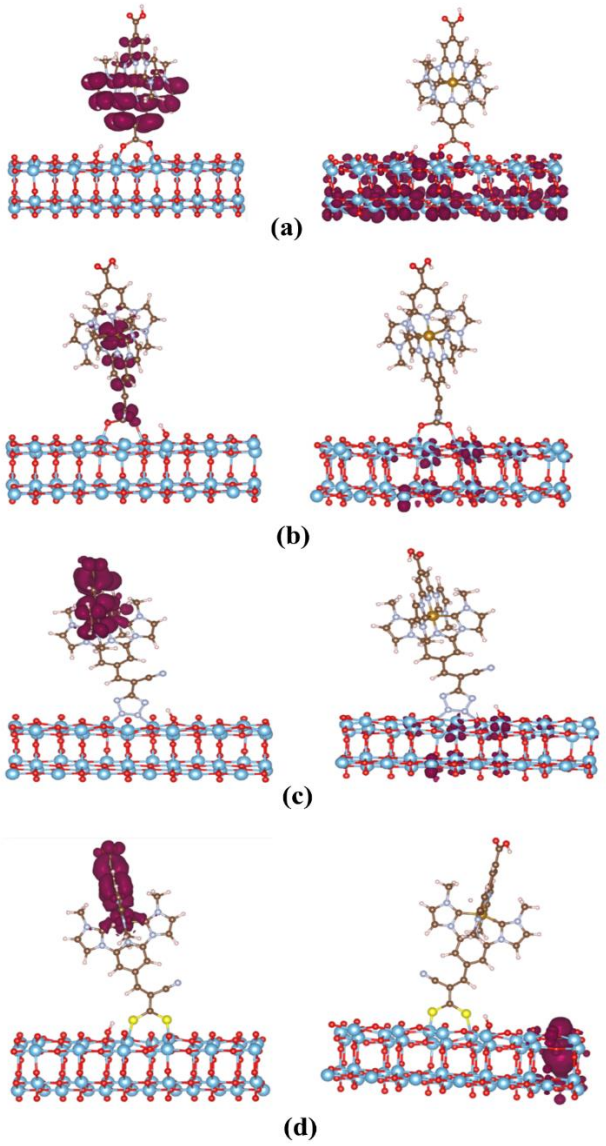

Figure 12. VBM and CBM isosurface plots for FD-TiO_2 (101) composites with (a) FD1, (b) FD2, (c) FD3, and (d) FD4

4. Conclusions:

In this work, we have made a comprehensive theoretical investigation of the Fe(II)-polypyridines based dyes with different anchoring groups to evaluate the photovoltaic

properties and kinetics of the IET process involving TiO2 as photoanode. Utilizing density functional theory (DFT) and time-dependent DFT calculations, structural, electronic, optical, and photovoltaic properties of Fe(II)-polypyridine based dyes are evaluated. Theoretical calculations showed that certain anchoring groups like cyanoacrylic acid and cyano triazole are capable of displaying a decent level of absorption-broadening abilities over the entire visible range of the solar spectrum enabling improved light harvesting capacity and driving force of electron injection than simple cyanoacrylic acid as anchor. Furthermore, the electron injection efficiency from the LUMOs of the dyes to the conduction band of TiO2 surface is improved with cyanoacrylic acid and cyano triazole anchors. The MO energy levels, and percentage of electron density data confirm that the presence of these anchoring groups, the LUMO states of the dyes become denser, which interacted strongly with the surface states of the semiconductor and thus the electron injection becomes faster for FD2 (τ=962fs) compared to the parent dye (τ=14.92 ps). These outcomes infer that thoughtful choice of anchor groups can improve the photovoltaic performances of the Fe(II)-polypyridine based dyes.

Conflicts of Interest

The author declares that there is no conflict of interest.

Data availability

Data is available upon request to the corresponding author.

Author contributions

Waleed S Alkhuraiji: Conceptualization of work, investigation of data, Resources, Writing - review & editing, Writing - original draft.

Funding Information

The author declared that no funding is received for the present work.

Acknowledgments

The authors sincerely acknowledge the computational resource support from King Khalid Military Academy (Ministry of National Guard), Govt. of Saudi Arabia and He is thankful to Prof. Kumaresh Ghosh at University of Kalyani, India.

References

1. Østergaard PA, Duic N, Noorollahi Y, Kalogirou S. Advances in renewable energy for sustainable development. Renewable Energy. 2023;219:119377, https://doi.org/10.1016/j.renene.2023.119377.
2. Mariotti N, Bonomo M, Fagiolari L, Barbero N, Gerbaldi C, Bella F. Recent advances in eco-friendly and cost-effective materials towards sustainable dye-sensitized solar cells. Green chemistry. 2020;22(21):7168-218, https://doi.org/10.1039/D0GC01148G
3. Docampo P, Guldin S, Leijtens T, Noel NK, Steiner U, Snaith HJ. Lessons learned: from dye-sensitized solar cells to all-solid-state hybrid devices. Advanced Materials. 2014;26(24):4013-30, https://doi.org/10.1002/adma.201400486
4. Roslan N, Ya'acob ME, Radzi MAM, Hashimoto Y, Jamaludin D, Chen G. Dye Sensitized Solar Cell (DSSC) greenhouse shading: New insights for solar radiation manipulation. Renewable and Sustainable Energy Reviews. 2018;92:171-86, https://doi.org/10.1016/j.rser.2018.04.095.
5. Zheng X, Liu C, Yan Y, Wang Q. A review of thermoelectrics research–Recent developments and potentials for

sustainable and renewable energy applications. Renewable and Sustainable Energy Reviews. 2014;32:486-503, https://doi.org/10.1016/j.rser.2013.12.053
6. Gao X, Kong C-p, Jia R, Jian W, Wang J, Bai F-q. Influence of one-dimensional TiO2 nanotube on interfacial electron transfer in dye-sensitized solar cells: Insights from theoretical investigation. Solar Energy. 2018;176:545-55, https://doi.org/10.1016/j.solener.2018.10.061
7. He J, Wang B, Chang S, Chen T. Ruthenium-based photosensitizers for dye-sensitized solar cells. Organometallics and Related Molecules for Energy Conversion. 2015:91-114, https://doi.org/10.1007/978-3-662-46054-2_4
8. Reynal A, Palomares E. Ruthenium polypyridyl sensitisers in dye solar cells based on mesoporous TiO2. European Journal of Inorganic Chemistry. 2011;2011(29):4509-26, https://doi.org/10.1002/ejic.201100516
9. Guo M, He R, Dai Y, Shen W, Li M, Zhu C. Electron-deficient pyrimidine adopted in porphyrin sensitizers: a theoretical interpretation of π-spacers leading to highly efficient photo-to-electric conversion performances in dye-sensitized solar cells. The Journal of Physical Chemistry C. 2012;116(16):9166-79, https://doi.org/10.1021/jp2109829
10. Housecroft CE, Constable EC. Solar energy conversion using first row d-block metal coordination compound sensitizers and redox mediators. Chemical Science. 2022;13(5):1225-62, https://doi.org/10.1039/D1SC06828H
11. Prajapat K, Dhonde M, Sahu K, Bhojane P, Murty VVS, Shirage PM. The evolution of organic materials for efficient dye-sensitized solar cells. Journal of Photochemistry and Photobiology C: Photochemistry Reviews. 2023;55:100586, https://doi.org/10.1016/j.jphotochemrev.2023.100586.
12. Woodhouse MD, McCusker JK. Mechanistic Origin of Photoredox Catalysis Involving Iron(II) Polypyridyl Chromophores. Journal of the American Chemical Society. 2020;142(38):16229-33. https://doi.org/10.1021/jacs.0c08389
13. Jakubikova E, Bowman DN. Fe (II)-polypyridines as chromophores in dye-sensitized solar cells: a computational perspective. Accounts of chemical research. 2015;48(5):1441-9, https://doi.org/10.1021/ar500428t
14. Mukherjee S, Bowman DN, Jakubikova E. Cyclometalated Fe (II) complexes as sensitizers in dye-sensitized solar cells. Inorganic chemistry. 2015;54(2):560-9, https://doi.org/10.1021/ic502438g
15. Yang M, Thompson DW, Meyer GJ. Charge-transfer studies of iron cyano compounds bound to nanocrystalline TiO2 surfaces. Inorganic chemistry. 2002;41(5):1254-62, https://doi.org/10.1021/ic011069q
16. Liu C. Modeling Dynamical Phenomena in Fe (II) Dyes and Dye-semiconductor Assemblies. North Carolina State University; 2019,
17. Curtin GM, Jakubikova E. Extended π-Conjugated Ligands Tune Excited-State Energies of Iron (II) Polypyridine Dyes. Inorganic Chemistry. 2022;61(47):18850-60, https://doi.org/10.1021/acs.inorgchem.2c02362
18. Monat JE, McCusker JK. Femtosecond excited-state dynamics of an iron (II) polypyridyl solar cell sensitizer model. Journal of the American Chemical Society. 2000;122(17):4092-7, https://doi.org/10.1021/ja992436o
19. Chergui M. Ultrafast photophysics of transition metal complexes. Accounts of chemical research. 2015;48(3):801-8, https://doi.org/10.1021/ar500358q
20. Bowman DN, Mukherjee S, Barnes LJ, Jakubikova E. Linker dependence of interfacial electron transfer rates in Fe (II)-polypyridine sensitized solar cells. Journal of Physics: Condensed Matter. 2015;27(13):134205, https://iopscience.iop.org/article/10.1088/0953-8984/27/13/134205
21. Wang Y, Chen B, Wu W, Li X, Zhu W, Tian H. Efficient solar cells sensitized by porphyrins with an extended conjugation framework and a carbazole donor: from molecular design to cosensitization. Angewandte Chemie. 2014;126(40):10955-9, https://doi.org/10.1002/anie.201406190
22. Biswas S, Pramanik A, Sarkar P. Origin of different photovoltaic activities in regioisomeric small organic molecule solar cells: the intrinsic role of charge transfer processes. The Journal of Physical Chemistry C. 2018;122(26):14296-303, https://doi.org/10.1021/acs.jpcc.8b02821
23. Nam Y, Lim JH, Ko KC, Lee JY. Photocatalytic activity of TiO2 nanoparticles: a theoretical aspect. Journal of Materials Chemistry A. 2019;7(23):13833-59, https://doi.org/10.1039/C9TA03385H
24. Ditchfield R, Hehre WJ, Pople JA. Self-consistent molecular-orbital methods. IX. An extended Gaussian-type basis for molecular-orbital studies of organic molecules. The Journal of Chemical Physics. 1971;54(2):724-8, https://doi.org/10.1063/1.1674902

25. Rassolov VA, Ratner MA, Pople JA, Redfern PC, Curtiss LA. 6-31G* basis set for third-row atoms. Journal of Computational Chemistry. 2001;22(9):976-84, https://doi.org/10.1002/jcc.1058
26. Hay PJ. Gaussian basis sets for molecular calculations. The representation of 3d orbitals in transition-metal atoms. The Journal of Chemical Physics. 1977;66(10):4377-84, https://doi.org/10.1063/1.433731
27. Miertuš S, Scrocco E, Tomasi J. Electrostatic interaction of a solute with a continuum. A direct utilizaion of AB initio molecular potentials for the prevision of solvent effects. Chemical Physics. 1981;55(1):117-29, https://doi.org/10.1016/0301-0104(81)85090-2
28. Cossi M, Barone V, Cammi R, Tomasi J. Ab initio study of solvated molecules: a new implementation of the polarizable continuum model. Chemical Physics Letters. 1996;255(4-6):327-35, https://doi.org/10.1016/0009-2614(96)00349-1
29. Frisch M. gaussian 09, Revision d. 01, Gaussian. Inc, Wallingford CT. 2009;201.
30. Becke AD. Density-functional thermochemistry. I. The effect of the exchange-only gradient correction. The Journal of chemical physics. 1992;96(3):2155-60, https://doi.org/10.1063/1.462066
31. O'boyle NM, Tenderholt AL, Langner KM. Cclib: a library for package-independent computational chemistry algorithms. Journal of computational chemistry. 2008;29(5):839-45, https://doi.org/10.1002/jcc.20823
32. Perdew JP, Burke K, Ernzerhof M. Generalized gradient approximation made simple. Physical review letters. 1996;77(18):3865, https://doi.org/10.1103/PhysRevLett.77.3865
33. Perdew JP, Chevary JA, Vosko SH, Jackson KA, Pederson MR, Singh DJ. Atoms, molecules, solids, and surfaces: Applications of the generalized gradient approximation for exchange and correlation. Physical review B. 1992;46(11):6671, https://doi.org/10.1103/PhysRevB.46.6671
34. Abuabara SG, Rego LG, Batista VS. Influence of thermal fluctuations on interfacial electron transfer in functionalized TiO2 semiconductors. Journal of the American Chemical Society. 2005;127(51):18234-42, https://doi.org/10.1021/ja055185u
35. Jakubikova E, Snoeberger III RC, Batista VS, Martin RL, Batista ER. Interfacial electron transfer in TiO2 surfaces sensitized with Ru (II)− polypyridine complexes. The Journal of Physical Chemistry A. 2009;113(45):12532-40, https://doi.org/10.1021/jp903966n
36. Sholl DS, Tully JC. A generalized surface hopping method. The Journal of chemical physics. 1998;109(18):7702-10, https://doi.org/10.1063/1.477416
37. Akimov AV, Prezhdo OV. Advanced capabilities of the PYXAID program: integration schemes, decoherence effects, multiexcitonic states, and field-matter interaction. Journal of chemical theory and computation. 2014;10(2):789-804, https://doi.org/10.1021/ct400934c
38. Guo Z, Liang W, Zhao Y, Chen G. Real-time propagation of the reduced one-electron density matrix in atom-centered orbitals: Application to electron injection dynamics in dye-sensitized TiO2 clusters. The Journal of Physical Chemistry C. 2008;112(42):16655-62, https://doi.org/10.1021/jp802007h ·
39. Zhang J, Zhang J-Z, Li H-B, Wu Y, Geng Y, Su Z-M. Rational modifications on champion porphyrin dye SM315 using different electron-withdrawing moieties toward high performance dye-sensitized solar cells. Physical Chemistry Chemical Physics. 2014;16(45):24994-5003, https://doi.org/10.1039/C4CP03355H
40. Lu T-F, Li W, Zhang H-X. Rational design of metal-free organic D-π-A dyes in dye-sensitized solar cells: Insight from density functional theory (DFT) and time-dependent DFT (TD-DFT) investigations. Organic Electronics. 2018;59:131-9, https://doi.org/10.1016/j.orgel.2018.05.005